LAWRENCE
LIVERMORE
NATIONAL
LABORATORY

UCRL-JRNL-228353

Achieving High Flux Amplification in a Gun-driven, Flux-core Spheromak

E. B. Hooper, D. N. Hill, H. S. McLean, C. A. Romero-Talamás, R. D. Wood

February 26, 2007

Nuclear Fusion

UCRL-JRNL-XXXXX

Achieving high flux amplification in a gun-driven, flux-core spheromak

E. B. Hooper, D. N. Hill, H. S. McLean, C. A. Romero-Talamás, R. D. Wood

Lawrence Livermore National Laboratory, Livermore CA 94551, USA

A new means of operating flux-core spheromaks with possibly increased stability, confinement and pulse length is analyzed by a resistive MHD model. High amplification of the bias poloidal flux, required to minimize ohmic losses, is achieved by reducing the bias rapidly in a plasma formed at a lower amplification. The plasma separatrix is predicted to expand and incorporate the removed bias flux maintaining the total poloidal flux within the spheromak's flux-conserving wall. MHD energy on open magnetic field lines is reduced, reducing magnetic fluctuation levels. A means of experimental verification is suggested that may point the way to fusion-relevant spheromaks.

PACS Numbers: 52.55.Ip 52.30.Cv

I. Introduction

The flux-core spheromak has a toroidal magnetic confinement geometry formed in an axisymmetric, simply-connected magnetic flux conserver. An applied (bias) poloidal flux and electric current from an electrode ("gun") thread the hole in the torus and are amplified by a dynamo effect, in principle to an arbitrary level [1], generating a steady component of the toroidal current in a nearly-axisymmetric magnetic geometry without the flux limits of a transformer. As discussed later, however, experiments and modeling find that amplification by the dynamo saturates at a low enough level that resistive losses in the open field line, edge plasma dominate the power balance of the spheromak. These losses must be reduced to a relatively low level for spheromaks to make attractive, high-temperature experiments or reactors. In addition to observations on the Sustained Spheromak Physics Experiment (SSPX) [2] which are discussed in more detail in this paper, saturation has also been seen in the Compact Toroid Experiment (CTX) [3], the Flux Amplification Toroid (FACT) [4], and the Spheromak Experiment (SPHEX) [5].

Resistive magnetohydrodynamic (MHD) modeling is used here to analyze a new method (*active bias-reduction*, ABR) of achieving high amplification following an initial low-amplification phase, thereby reducing the resistive losses on open field lines and potentially offering a significant step towards fusion-quality spheromak plasmas. ABR extends helicity injection from a coaxial gun (CHI) [6], e.g. as used in SSPX [2, 7] to form spheromak plasmas. The MHD code used in this study, NIMROD [8], has been benchmarked against SSPX [9, 10] which is researching a range of physics including flux and current amplification [2], the role of magnetic fluctuations in the formation and confinement of the spheromak

plasma [11], and magnetic reconnection generating the conversion of injected toroidal flux into poloidal flux [12]. For a review of previous spheromak research see Jarboe [6] and references therein.

The spheromak has a number of features which make it a potentially attractive fusion-energy device. An axisymmetric, simply-connected flux conserver surrounds the plasma with no toroidal-field coils along the magnetic axis, yielding a compact system so a spheromak should be easier to maintain than the tokamak and stellarator. The use of helicity injection to drive and sustain a toroidal current without a transformer provides additional simplicity, including a natural divertor. The trade-off is an increase in physics complexity. Furthermore, increasing and sustaining current parallel to the magnetic field in the spheromak requires that magnetic surfaces be open at least part of the time [13], with significant consequences for energy confinement which may require separation of the current drive and confinement phases in a reactor [14]. The spheromak current and flux will decay during the confinement phase as the dynamo is turned off, so it will likely be necessary to rebuild them periodically using a dynamo pulse. Experiments in SSPX exploring the physics of helicity injection into a slowly-decaying spheromak [15] to rebuild the plasma thus complement the present flux-amplification concept by developing a technique to extend the plasma duration.

II. Flux Amplification in SSPX

A flux-core spheromak for a high-temperature confinement experiment or reactor will require a bias poloidal flux amplification of 50-100, primarily to minimize the volume of open field lines to keep ohmic losses in the edge from

dominating the power balance [16]. Consider the two SSPX MHD equilibria in Fig. 1. These were generated by solving the Grad-Shafranov equation using the Corsica code [7] in the SSPX geometry, which is used in this study as spheromaks in it are well characterized. The equilibrium in Fig. 1a is a fit to an experimental discharge with $\lambda = \mu_0 \mathbf{j} \cdot \mathbf{B} / B^2$ assumed spatially constant but chosen to optimize the fit to experimental measurements; **j** is the current density, and **B** is the magnetic field. The equilibrium in Fig. 1b was found by reducing the bias flux at fixed $\lambda_g = \mu_0 I_g / \Psi_g$, with I_g the gun current and Ψ_g the effective applied bias flux (which is also the flux on the separatrix), and fixed Ψ_0, the poloidal flux between the magnetic and geometric axes. The cross section area of the edge plasma, between the separatrix and geometric axis or wall, scales inversely as the flux amplification, Ψ_0 / Ψ_g.

The edge fieldline connections to material surfaces result in a low (~ 30 eV) edge electron temperature with correspondingly large ohmic losses. (Helicity-injection techniques that drive current on open fieldlines outside the separatrix [17] may yield higher temperatures.) Increasing the flux amplification at fixed λ_g thus reduces the ohmic power loss proportionally. High amplification is essential for efficient operation of future spheromak experiments.

Experimental results to date typically achieve flux amplifications of about 3-4, although up to 6 has been obtained. Experimental results are compared with resistive MHD simulations [14] in Fig. 2. The current amplification is defined as the ratio of toroidal current in the flux conserver to the gun current and is approximately 1/2 the flux amplification. The observed threshold dependence on λ_g is consistent with the Kruskal-Shafranov condition for instability of a

plasma column, which is $\lambda_g > 4\pi/L$ with L the effective length of the column. The numerical factor will be different in SSPX; it is reduced if one or both ends of the column are not line-tied [18], and the effective length of the column in SSPX is longer than the flux-conserver height due to the coaxial gun, so there is semi-quantitative agreement of this simple condition with experiment, as in other spheromaks [5, 19].

The detailed reasons for the flux amplification saturation at fixed λ_g are not well understood. Modeling of the column mode in SPHEX [20] suggests that the coupling to the spheromak limits its amplitude and can even stabilize the mode intermittently, but full stabilization has not been observed in SSPX or its simulations. In any event, it is clear that the gun voltage and thus the helicity injection rate, $\dot{K}_{inj} = 2\Psi_g V_g$, are determined by λ_g. In experiments it is seen that the magnitude of the gun voltage increases with λ_g [14, 21]. The voltage spikes generated by the reconnection events, seen clearly in simulations [12], have higher amplitude and a faster repetition rate at the higher λ_g in both simulation and experiment. Figure 3 shows the gun voltages and the energy in the $n = 1$ mode for two of the simulations used in Fig. 2. The greater rate of helicity injection at higher λ_g results in greater (but saturated) magnetic energy in the flux conserver as noted in the caption to Fig. 3.

In principle, we can obtain high flux amplification by going to high λ_g. Extrapolating Fig. 2 to an amplification of 50 yields $\lambda_g = 96$ m^{-1}; at bias fluxes of 30-50 mWb, typical of good operation in SSPX, this requires $I_g = 2.3$-3.8 MA. These very high gun currents (and powers) would damage the gun and generate significant impurities, and are not very practical. Furthermore, solutions of the

Grad-Shafranov equation for SSPX [7], fitted to experimental magnetic probe measurements, show that a large value of λ on the edge of the mean-field (azimuthally-averaged) spheromak results in a large λ-gradient with a deep minimum on the (mean-field) magnetic axis. The corresponding safety factor, q, crosses unity between the separatrix and the magnetic axis if the spheromak is driven strongly enough, and would likely drive strong n=1 interior oscillations if the nearly symmetric state were a good approximation in this state. In fact, detailed probe measurements in SPHEX [5, 22] show a highly nonaxisymmetric, nonlinear structure develops in strongly driven spheromaks. Although experiments have never reached high amplification, this large departure from symmetry suggests that the resulting spheromak would be of poor quality.

III. Flux amplification using Active Bias Reduction: 2D model

Experiments and simulations thus suggest that it will be very difficult to obtain high flux amplification simply by driving the gun for a long time at high current. Instead, we consider an alternative approach, ABR. A high current spheromak is formed, e.g., as in conventional CHI. The bias flux and gun current are then reduced together to low values while maintaining their ratio constant, thus maintaining the edge boundary condition in λ needed for global stability. 3D simulations below show that the total poloidal flux and toroidal current in the flux-conserver remain approximately constant during this process so the flux amplification increases while the ohmic edge losses decrease. The poloidal flux and current within the spheromak separatrix increase as it expands to include more of the flux-conserver volume. An additional advantage will be seen to be a

significant reduction of the amplitude of MHD modes driven by the gun current. As a result, the spheromak plasma is better confined and hotter in the subsequent, high-temperature phase [11] than in the absence of ABR.

Before describing the resistive, 3D MHD simulation of ABR, consider an axisymmetric approximation. The highly conducting flux conserver in the present experiment will not allow the bias magnetic flux to be reduced on the discharge time scale, but we assume that modifications, such as a vertical cut in the gun wall, allow the axisymmetric bias flux to be changed rapidly. The gun current and bias flux are changed together, so that λ_g is constant during the process. In experiments and simulations the total poloidal flux, Ψ_0, is generated from injected toroidal flux by reconnection events associated with the dynamo [12], but we assume that there is no dynamo during the bias flux change so the poloidal flux on the magnetic axis of the spheromak is constant. (Resistive MHD simulations, discussed in the following section, guided this assumption.)

An initial equilibrium was shown in Fig. 1 along with the result of increasing the flux amplification by a factor of 10 at constant λ_g. The scaling of spheromak parameters during this change is shown in Fig. 4. Note that the magnetic energy and helicity decrease somewhat as the gun flux and current are reduced at constant total poloidal flux. During a discharge the injected power and rate-of-helicity are $\dot{W}_{inj} = I_g V_g$ and $\dot{K}_{inj} = 2\Psi_g V_g$, so the part of the gun voltage, V_g, generating stored energy and helicity will reverse sign. (The total voltage includes ohmic losses on open field lines and, in the experiment, a drop across the sheath [21].) The toroidal current also drops slightly. We can estimate the vertical magnetic field on the geometric axis as $\sim\mu_0 I_T f/2\pi R_0$ where f=1 assumes

that the toroidal current is concentrated at the magnetic axis, and f~1 results from a distributed current, so $I_T \approx$ constant implies that the vertical field near the geometric axis is approximately constant during the process. The minimum radius of the separatrix then scales as $\Psi_g^{1/2}$, close to that seen in the calculation. The edge ohmic losses decrease approximately proportional to the gun current and thus proportional to Ψ_g, a factor of 10 in this example.

IV. Flux amplification using Active Bias Reduction: 3D simulation

Resistive MHD modeling is used for a 3D simulation of ABR with the spheromak poloidal flux calculated self consistently. The simulation used similar parameters to those in Refs. 10 and 12 including high parallel thermal conductivity and a perpendicular thermal conductivity coefficient similar to measurements in SSPX [11], toroidal modes 0-5, and kinetic viscosity of 1000 m^2/s. Comparisons of simulations with experiment find that these give a reasonably good approximation to observations for many of the important physics parameters, as discussed in the previous publications.

A discharge is established at constant bias flux, resulting in the azimuthally-averaged equilibrium shown in Fig. 5a. The bias and gun current are then reduced over 1 ms with the time dependence shown in Fig. 6a, resulting in the equilibrium in Fig. 5b. Fig. 6b shows the gun voltage and Fig. 6c the toroidal current and total energy in the flux conserver throughout this time. The total energy, which is primarily in the magnetic field, drops during ABR consistent with the reduction in power input.

The azimuthally-averaged poloidal flux surfaces at the start and end of the ramp down can be compared with those in Fig. 1; the minimum radius of the separatrix goes from 0.075 m to 0.02 m, again in agreement with the approximate $\Psi_g^{1/2}$ scaling. The detailed magnetic structures in the coaxial gun differ, but otherwise the behavior is nearly the same. The poloidal flux on the magnetic axis drops a bit, by an amount consistent with resistive decay of the toroidal current. As was assumed in the 2D model, the spheromak separatrix expands to include most of the initial edge flux.

The NIMROD simulation includes the resistive voltage drop although not a sheath voltage, and the net voltage is positive throughout most of the pulse although its sign reverses when the gun current and flux are changing the most rapidly. At the beginning of the pulse, the resistive voltage drop is $V_g = I_g \eta \ell / A$, where η is the resistivity and ℓ and A are appropriate averages of the current path length and edge area. At 25 eV, $\ell \approx 1$ m, and $A \approx 0.03$ m^2, $V_g \approx 100$ V, in rough agreement with Fig. 5b. The voltage "jumps" at about 4.9 ms result when the position at which the separatrix connects to the gun wall switches from high in the gun (Fig. 5a) to low in the gun (Fig. 5b). The separatrix X-point moves to the gun wall near an X-point in the bias magnetic field; the separatrix in Fig. 5b shows a break at this location, near the gun wall just below 0.4 m.

Following ABR the simulation is continued to $t \approx 10$ms with the gun current reduced in the simulation by a constant factor of 12.9. The gun voltage is approximately constant at 60 V during this time and there is no indication of reconnection events or helicity drive of the spheromak. The azimuthally-averaged and $n = 1$ magnetic energies are compared in Fig. 7 with those in the

absence of ABR; the averaged energy differs little but the $n = 1$ energy is significantly reduced. This is consistent with a qualitative picture in which the column mode is coupled to the spheromak which is stabilized to the tilt and shift (n=1, m=1) modes by the flux conserver geometry. Although the Kruskal-Shafranov condition for an isolated column has not been affected as λ_g is constant, the free energy available to drive the mode is reduced at lower gun current, thereby likely yielding the lower amplitude. Indeed, this low amplitude suggests that the mode is stable and driven only by mode coupling during this time. After about 1 ms the amplitude of the n=1 column mode increases, but its amplitude is still significantly reduced from the original value, by ~35 in this example.

The energies in modes 2-5 are compared in Fig. 8 for the ABR and non-ABR simulations. They are generally reduced in the latter case. After about 8 ms in the non-ABR simulation there are strong 2/3 magnetic islands near the magnetic axis and a significant volume of stochastic magnetic fieldlines which allow large thermal losses. The reduced activity in the ABR case allows a larger volume of good magnetic surfaces resulting in a calculated peak- electron temperature in the simulation of $T_e \approx 170$ eV, two to three times that in the non-ABR example.

V. Experimental considerations and summary

Experiments studying ABR will require a flux conserver that differs from those presently in use to allow for rapid changes in magnetic flux demanded by this new scenario. An example of a possible design is shown in Fig. 9. Bias poloidal flux enters the flux conserver through the gap in the gun at the top and exits through the hole in the bottom. The external coils are adjusted such that the

shape of the outer vacuum flux surface closely follows the contour of the flux conserver. For the flux to be changed on a fast (millisecond) time, the walls of the gun will have to have a vertical slot or the magnets will need to be inside the gun walls. As the magnetic energy within the flux conserver decreases only slightly during ABR, the magnetic energy to be removed is that in the gun and exit volumes; for each, $W_0 \approx \Psi_g^2 / 2\mu_0 \pi a^2 L$ with a and L the characteristic radius and length of a section. The voltage required is $V \approx 2W_0 / I_0 \tau$, with τ the characteristic ABR time. At Ψ_g = 50 mWb, a = 0.2 m, and L = 0.5m, W_0 = 16 kJ; if I_0 = 1 kA and τ = 1 ms, $V \approx$ 15 kV. Detailed design would undoubtedly change these, but the numbers given here suggest that the eventual parameters will be reasonable for an experiment although careful bias-coil design will be needed. A larger flux conserver may have higher T_e, allowing a slower ABR time, although detailed modeling will be required to explore this scaling.

ABR is also consistent with the control of the tilt and shift modes by feedback stabilization such as an "intelligent" wall [23] rather than by a highly conduction flux conserver. Recent experimental studies in the reversed-field pinch with a thin, resistive wall demonstrate successful active stabilization of non-resonant resistive wall modes and locking of resonant tearing modes over the duration of the discharge [24]. Detailed examination of this physics in the spheromak is beyond the present study.

In conclusion, both experiments and simulations suggest that it will be very difficult to achieve high flux and current amplification in a conventional, helicity-injected spheromak. The injection would have to be driven extremely "hard" (with the gun current >> the threshold in λ_g) likely damaging electrodes and

perhaps generating such a high degree of asymmetry that a good spheromak cannot be formed. We are thus motivated to find a new approach to achieving flux amplification. The present concept, Active Bias Reduction, is considered in that context.

Resistive MHD modeling of flux amplification in a flux-core spheromak predicts that ABR has additional benefits. The plasma stability is improved with reduced ohmic losses on open field lines. The amplitudes of resonant magnetic modes are reduced, resulting in improved magnetic surfaces and reduced thermal losses. Such an approach would also be consistent with an advanced spheromak experiment, e.g. using feedback stabilization rather than a highly-conducting flux conserver.

The modeling also indicates that an axisymmetric, quasi-static model using the Grad-Shafranov equation can be used to explore the MHD evolution of these plasmas, allowing fast exploration of experimental options. Resistive MHD modeling will be important for optimization, e.g. by exploring the sensitivity of stability to the value of λ_g following ABR. The results obtained in this report suggest that ABR is a mechanism for achieving high flux amplification, one of the requirements for significant progress towards a fusion-quality plasma in a spheromak.

Acknowledgements

The approach to flux amplification analyzed here arose from discussions with T.K. Fowler. C.R. Sovinec's guidance was essential in modifying NIMROD for the ABR calculations. Careful reading and comments by B.I. Cohen and E.J. Synakowski are gratefully acknowledged. Discussions with many colleagues,

including L. L. LoDestro, L. D. Pearlstein, and D. D. Ryutov, have helped form our understanding of spheromaks. This work was performed under the auspices of the U.S. Department of Energy under contract W7405-ENG-48 at the University of California Lawrence Livermore National Laboratory.

References

1. J.B. Taylor and M.F. Turner, Nucl. Fusion **29**, 219 (1989).
2. R.D. Wood, D.N. Hill, E.B. Hooper, S. Woodruff, H.S. McLean, , B.W. Stallard, Nucl. Fusion **45**, 1582 (2005).
3. T. R. Jarboe, I. Henins, A. R. Sherwood, C. W. Barnes, and H. W. Hoida, Phys. Rev. Lett., **51**, 39 (1983).
4. M. Nagata, T. Kanki, T. Matsuda, S. Naito, H. Tatsumi, and T. Uyama, Phys. Rev. Lett. **71**, 4342 (1993)
5. R. C. Duck, P. K. Browning, G. Cunningham, S. J. Gee, A. al-Karkhy, R. Martin, and M. G. Rusbridge, Plasma Phys. Control. Fusion **39**, 715 (1997).
6. T. R. Jarboe, Plasma Phys. Control. Fusion **36**, 945 (1994).
7. E.B. Hooper, L.D. Pearlstein, R. H. Bulmer, Nucl. Fusion **39**, 863 (1999).
8. C. R. Sovinec, T. A. Gianakon, E. D. Held, S. E. Kruger, D. D. Schnack, and the NIMROD Team, Phys. Plasmas **10**, 1727 (2003).
9. C. R. Sovinec, B. I. Cohen, G. A. Cone, E. B. Hooper, and H. S. McLean, Phys. Rev. Letters **94**, 035003 (2005).
10. B. I. Cohen, E. B. Hooper, R. H. Cohen, D. N. Hill, H. S. McLean, R. D. Wood, S. Woodruff, C. R. Sovinec, and G. A. Cone, Phys. Plasmas **12**, 056106 (2005).
11. H. S. McLean, R. D. Wood, B. I. Cohen, E. B. Hooper, D. N. Hill, J. M. Moller, C. Romero-Talamas, S. Woodruff, Phys. Plasmas **13**, 056105 (2006).
12. E. B. Hooper, T. A. Kopriva, B. I. Cohen, D. N. Hill, H. S. McLean, R. D. Wood, S. Woodruff, C. R. Sovinec, Phys. Plasmas **12**, 092503 (2005).
13. A. H. Boozer, Phys. Fluids B **5**, 2271 (1993).

14. E. B. Hooper, B. I. Cohen, D. N. Hill, L. L. LoDestro, H. S. McLean, C. A. Romero-Talamás, R. D. Wood, J. Fusion Energy (to be published); published on line at http://www.springerlink.com/content/4u8640028j835487; doi: 10.1007/s10894-006-9065-y (2007).
15. S. Woodruff, B. W. Stallard, H. S. McLean, E. B. Hooper, R. Bulmer, B. I. Cohen, D. N. Hill, C. T. Holcomb, J. Moller, and R. D. Wood, Phys. Rev. Letters **93**, 205002 (2004).
16. R.L. Hagenson and R. A. Krakowski, Fusion Techn. **8**, 1606 (1985).
17. P.E. Sieck, T.R. Jarboe, V. A. Izzo, W.T. Hamp, B.A. Nelson, R.G. O'Neill, A.J. Redd, and R.J. Smith, Nucl. Fusion **46**, 254 (2006).
18. D. D. Ryutov, I. Furno, T. P. Intrator, S. Abbate, and T. Madziwa-Nussinov, Phys. Plasmas **13**, 032105 (2006).
19. W. C. Turner, G. C. Goldenbaum, E. H. A. Granneman, J. H. Hammer, C. W. Hartman, D. S. Prono, and J. Taska, Phys. Fluids **26**, 1965 *1983).
20. D. Brennan, P. K. Browning, R. A. M. Van der Linden, A. W. Hood, and S. Woodruff, Phys. Plasmas **6**, 4248 (1999).
21. B. W. Stallard, E. B. Hooper, S. Woodruff, R. H. Bulmer, D. N. Hill, H. S. McLean, R. D. Wood, and the SSPX Team, Phys. Plasmas **10**, 2912 (2003).
22. S. Woodruff and M. Negata, Plasma Phys. and Control. Fusion **44**, 2539 (2002).
23. C. M. Bishop, Plasma Phys. Controlled Fusion **31**, 1179 (1994).
24. P. R. Brunsell, M. Kuldkepp, S. Menmuir, M. Cecconello, A. Hedqvist, D. Yadikin, J. R. Drake, and E. Rachlew, Nucl. Fusion **46**, 904 (2006).

Figure Captions

Fig. 1. (a) Spheromak (SSPX) axisymmetric equilibrium with $\lambda_g = 9.3$ m^{-1} and flux amplification 3.3. (b) Axisymmetric equilibrium with reduced bias flux at fixed λ_g yielding flux amplification = 32.4. The flux conserver surrounds the plasma, and the bias flux is generated by the external coils.

Fig. 2. Flux amplification in the SSPX experiment and simulations. The experimental results are the ratio of the peak flux achieved to the applied bias flux. In most of these experiments the gun-current pulse is not long enough for the flux amplification to saturate, so the data is a lower bound on the amplification. A Bessel-function model is used to calculate the flux from magnetic field measurements in the experiment. The simulations (labeled "NIMROD") use a long, constant-current pulse and reach saturation.

Fig. 3. Total magnetic energy from NIMROD simulations within the flux conserver for the $n = 1$ column mode (upper figure) and gun (cathode) voltage (lower figure) during sustainment at $\lambda_g = 20.3$ m^{-1} ("spiky" traces) and 13.6 m^{-1} ("smooth" traces). The energies in the $n = 0$ (axisymmetric) modes are 370 kJ and 82 kJ, respectively.

Fig. 4. Flux amplification scaling in the axisymmetric model of (a) magnetic energy, W, and helicity, K, and (b) toroidal current, I_T, and minimum separatrix radius, r_{min}.

Fig. 5. Poloidal flux (toroidally-averaged) surfaces from a 3D resistive MHD simulation of bias flux reduction with a flux amplification change from 5.0 to 64.4; λ_g = 13.6 m^{-1}. (a) Initial equilibrium. (b) Equilibrium at the end of the flux reduction.

Fig. 6. (a) Ramp-down of gun current, I_g, (b) gun (cathode) voltage, V_g, (c) magnetic energy, W, and toroidal current, I_T; note the suppressed zeros in (c).

Fig. 7. Magnetic energy in the n=0 (axisymmetric) and n=1 modes with (solid lines) and without ABR (dashed lines). λ_g is constant (13.6 m^{-1}) during both evolutions.

Fig. 8. Mode energies in simulations with and without ABR.

Fig. 9. Preliminary design for a new flux conserver and gun. Flux amplification = 41.

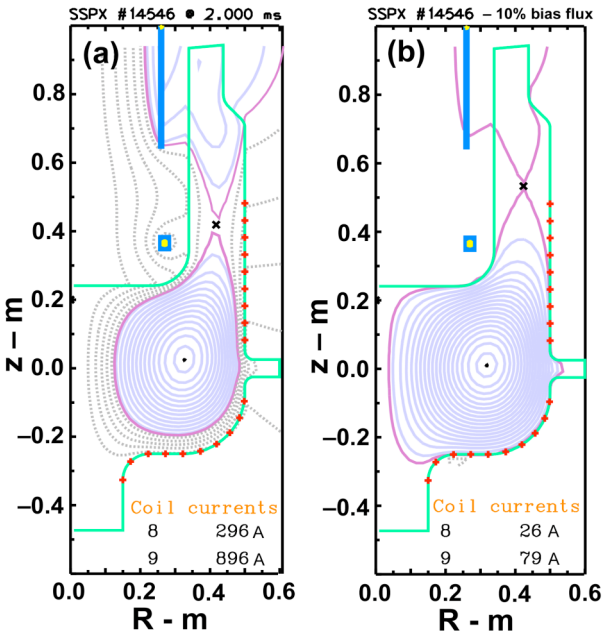

Hooper, et al., Fig. 1

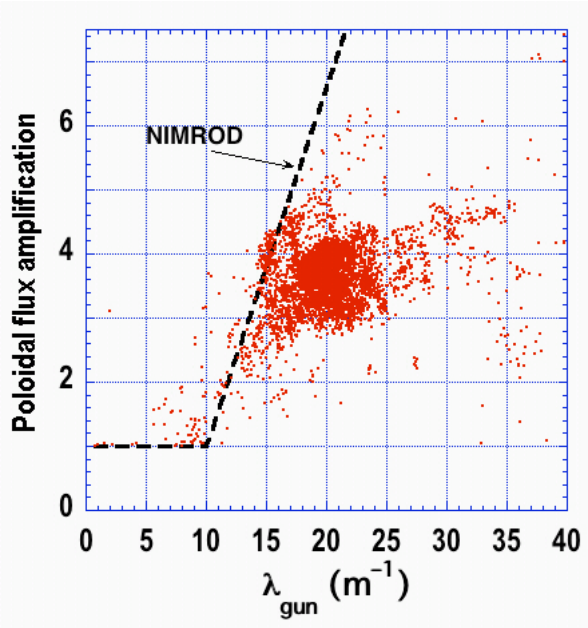

Hooper, et al., Fig. 2

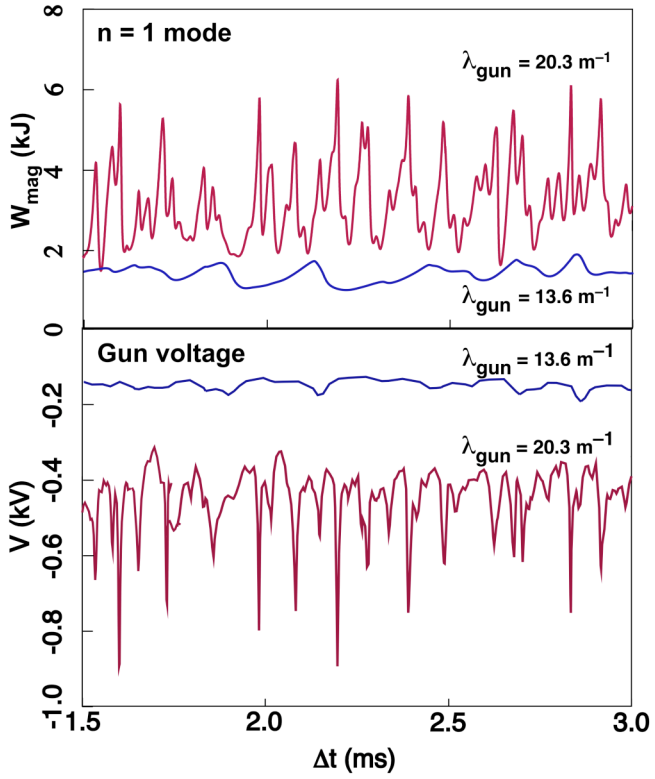

Hooper, et al., Fig. 3

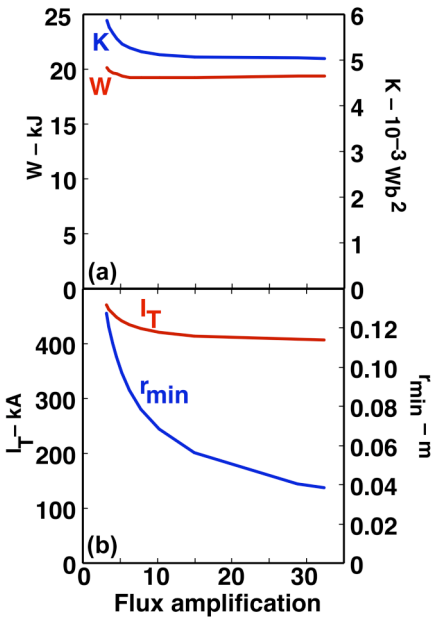

Hooper, et al., Fig. 4

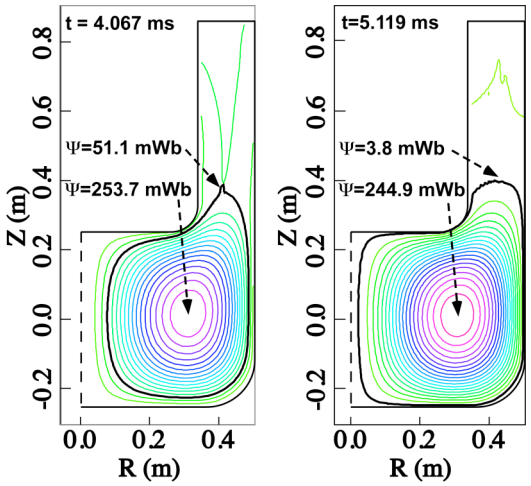

Hooper, et al., Fig.5

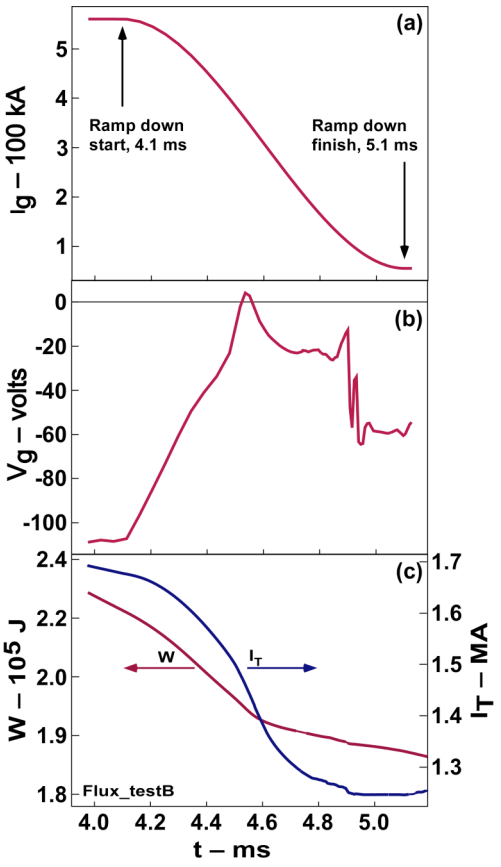

Hooper, et al., Fig. 6

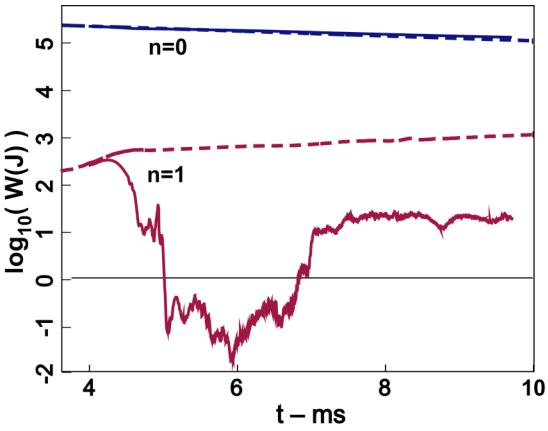

Hooper, et al., Fig. 7

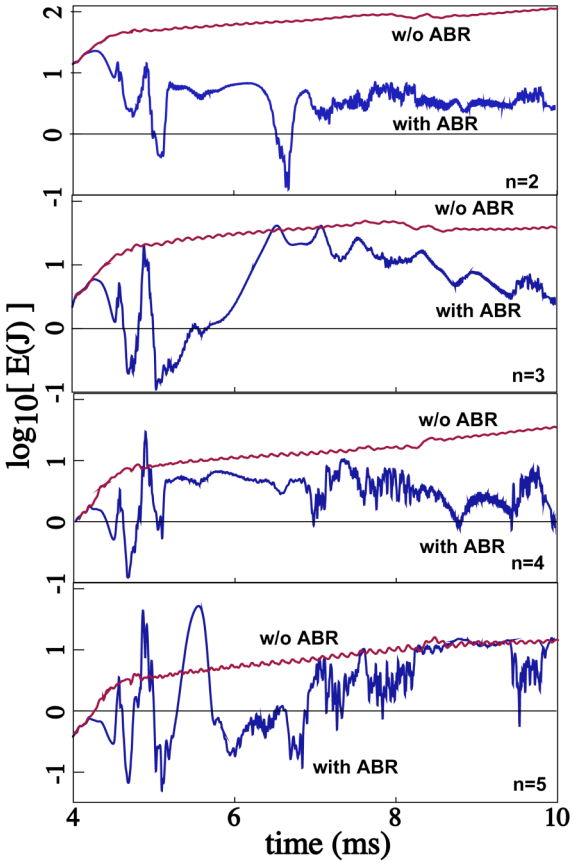

Hooper, et al., Fig. 8

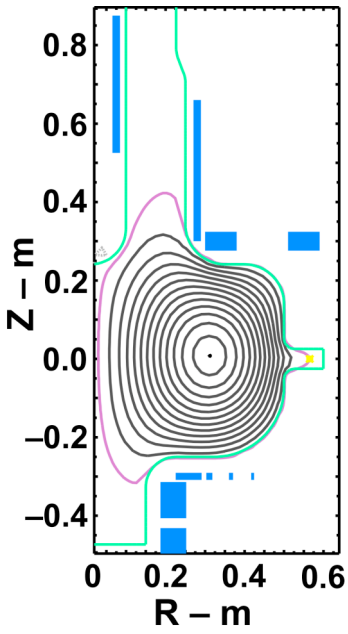

Hooper, et al., Fig. 9